Technoscience Journal for Community Development in Africa 4 (2025) 105–118
ISSN 2659-0573

Research Article

Design, fabrication, and performance analysis of a locally sourced hot-air balloon for high-temperature environments

Taofiq Omoniyi Amoloye[1*], Francis Ayomide Adedeji[2], Abdulfatai Olanrewaju Sulaiman[1], Abdulbaqi Jinadu[1], Olalekan Adebayo Olayemi[1]

[1]Department of Aeronautical and Astronautical Engineering, Kwara State University, Malete, Nigeria
[2]Department of Aeronautical and Astronautical Engineering, Afe Babalola University, Ado-Ekiti, Nigeria

Abstract: This research focuses on addressing the difficulty of manufacturing low-cost aerial platforms in developing regions by fabricating a functional hot-air balloon in Ilorin, Nigeria, with the exclusive use of indigenous materials. The methodology involved the use of polyester and Teru fabrics, developed from a novel Acrylic- Polyvinyl Acetate (PVA) sealing method and a locally sourced borax-boric acid fire retardant. Quantitative analysis of the components shows that the treated fabric attained an 80-85% air permeability reduction rate while the burner system achieved a 62% heat target output. The analysis also indicated an underestimated significant buoyancy penalty of over 12% resulting from high ambient temperatures (35°C). In conclusion, this study successfully shows the viability of utilizing local materials for functional aerospace vehicle components, developing a vital methodological framework. Hence, it provides needed performance data for future low-cost designs in high-temperature environments.

Keywords: Low-cost aerospace, Appropriate technology, Local materials, High-temperature operations, Engineering education.

1. Introduction

Hot-air balloons have a storied history and play a significant role in both the evolution of human flight and contemporary engineering applications. The origins of ballooning can be traced back centuries, with early forms, such as sky lanterns used in Buddhist ceremonies in East Asia, paving the way for later innovations. However, it was in 1783 that the first officially recognized manned lighter-than-air flight was achieved in Paris by the Montgolfier brothers, a milestone that predates the first powered heavier-than-air flight in America by more than a century (Barak & Raz, 2000; Korawutwiwat et al., 2022).

This pioneering achievement laid the groundwork for the development of various types of balloons, each leveraging the principle of buoyancy. When air is heated, it becomes less dense than the cooler surrounding air, generating an upward lifting force. Although early balloon designs sometimes used hydrogen for its superior lift properties, the inherent flammability of hydrogen led to significant safety concerns. As a result, safer alternatives, such as hot-air systems, where heated air alone produces lift, and the use of helium, a nonflammable gas, were explored, despite challenges related to cost and availability (Nordlie et al., 2014).

From a technical perspective, the design of a hot-air balloon revolves around three primary components: the envelope, the burner system, and the basket as shown in Fig. 1. The envelope is typically constructed from lightweight yet durable materials (such as rip-stop nylon or treated polyester) and is segmented into longitudinal sections known as gores. These gores are often reinforced with load tapes to distribute structural stress evenly and maintain the balloon's shape and integrity. In areas near the heat source, fire-resistant materials like Nomex are

* Corresponding author
Email: taofiq.amoloye@kwasu.edu.ng

KWASU PRESS AND PUBLISHING

employed to reduce the risk of damage. Meanwhile, the burner, which is usually fueled by propane, provides the necessary heat to lower the density of the air within the envelope, and the basket supports both the payload and control apparatus (Daidzic, 2021).

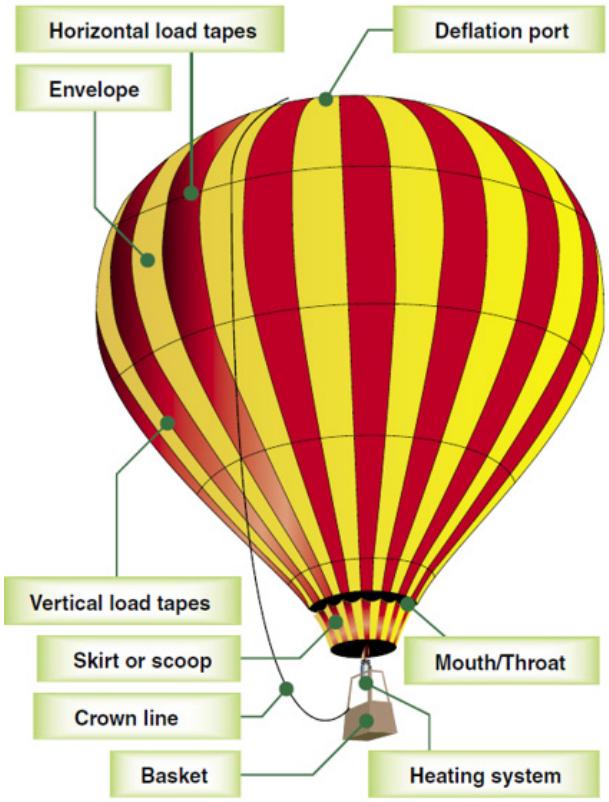

Figure 1: The basic part of a hot-air balloon (FAA, 2008)

Operational control of a hot-air balloon is inherently straightforward yet deeply reliant on natural forces. To ascend, the pilot increases the internal temperature using the burner, thereby enhancing buoyancy; descent is achieved by allowing the air to cool or by releasing hot air through a vent. Lateral movement is predominantly dictated by wind direction, making accurate meteorological data crucial for effective flight management.

Beyond their historical and technical significance, hot-air balloons have evolved to serve diverse modern applications. They are used not only in recreational activities, providing breathtaking aerial views in tourist destinations such as Cappadocia, and also some iconic landscapes in Africa which include the Serengeti in Tanzania and the Maasai Mara in Kenya (Atioğlu, 2021), but also as platforms for scientific research, where they offer unique opportunities to collect atmospheric data such as wind speeds and temperature profiles, essential for meteorological studies and climate research (Bruijn et al., 2016; Doerenbecher et al., 2016; Bruijn et al., 2023).

A review of the extant literature reveals a significant body of work on hot-air balloon technology, which can be broadly categorized into three areas: historical and technical foundations, modern scientific applications, and analyses of challenges in developing regions. The foundational principles of buoyancy and balloon design are well-established in handbooks and technical literature FAA (2008), Daidzic (2021), with recent scholarly work focusing on mathematical modeling of flight performance (Daidzic, 2021) and the evaluation of advanced materials for specialized applications like high-altitude solar balloons (Korawutwiwat et al., 2022). Furthermore, the role of balloons as platforms for atmospheric research and data collection is well-documented, particularly in mid-latitude regions (Bruijn et al., 2016; Bruijn et al., 2023; Doerenbecher et al., 2016).

While hot-air balloon technology is mature, its application in resource-constrained environments with challenging climates remains under-explored. Extensive details of this case study can be found in the publication by Amoloye (2014). Studies on aerospace development in emerging economies often highlight systemic challenges such as inadequate infrastructure, limited regulatory frameworks, and evolving safety standards (Mahto, 2018).

However, critical gaps remain in the translation of this high-level analysis into practical, ground-level engineering solutions. Specifically, there is a profound lack of scholarly work that:

1. Empirically evaluates the performance of non-standard, locally sourced materials (e.g., common textiles, alternative sealants) against the rigorous demands of aerodynamic design and thermal management.

2. Provides quantitative data on the performance penalties and necessary design adaptations for operating lighter-than-air systems in high-ambient-temperature, high-humidity environments like West Africa.

3. Develops and validates a replicable methodology for the indigenous fabrication of functional aerial vehicles using accessible tools and expertise.

This gap represents a missed opportunity for sustainable development and technological self-reliance. Therefore, this study aims to address this gap by moving beyond a theoretical discussion of challenges into the empirical realm of material science, adaptive design, and climate-specific performance analysis.

2. Materials and methods

The design of the hot-air balloon is fundamentally based on the principles of buoyancy, the ideal gas law, and heat transfer which are presented in Equations (1) – (3). These equations encapsulate the mathematical framework used in this case study.

$$\text{Buoyancy force} = (\text{Density of cold Air} - \text{Density of warm air}) \times \text{Volume of envelope.} \quad (1)$$

$$P = \rho R_{gas}\ T \quad (2)$$

$$Q_{ConvExt} = HC_{external} \times A_{effective} \times (T_{ambient\ air} - T_{envelope\ air}) \quad (3)$$

In Equations (2) and (3), P is the pressure, ρ is the density, R_{gas} is the universal gas constant, T is the temperature, $Q_{ConvExt}$ is the total amount of external convective heat transfer, $HC_{external}$ is the external convective heat transfer coefficient, and $A_{effective}$ is the effective surface area.

2.1. Design process

The design and construction of the hot-air balloon were executed through a cyclical, iterative engineering process. Each cycle starts from the brief (the details concerning the research or design to be done) as seen in Fig. 2., encompassing conceptualization (design ideas), prototyping, testing, and refinement, provided valuable feedback that guided subsequent improvements in design, material selection, and overall construction.

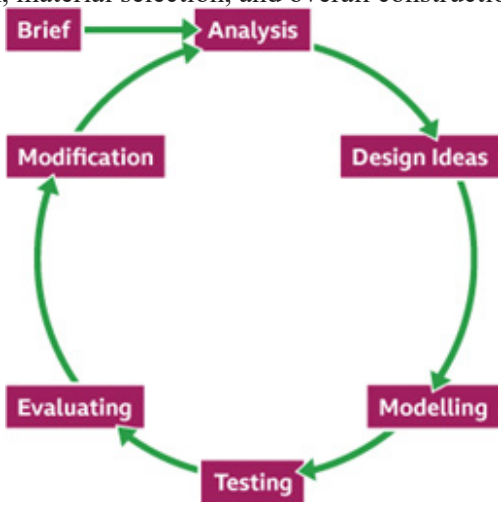

Figure 2: The engineering iterative design process (BBC 2023)

2.2. Design calculations

The design is based on Archimedes' principle, which dictates that a hot-air balloon must generate a buoyant force (expressed in mass) that exceeds the combined weight of its payload, structure, and other components.

2.2.1. Buoyancy and envelope volume

A body immersed in a fluid experiences a buoyant force equal to the weight of the displaced fluid. For our balloon, Equation (4) shows this relation.

$$Buoyancy\ force = Mass\ of\ cold\ air - Mass\ of\ warm\ air \quad (4)$$

With equal gravitational acceleration, we define buoyancy forces as Equation (1).

Now the weight of the parts of the hot air balloon must not exceed the buoyancy force. Otherwise, the balloon will not rise. From Equation (1), it can be seen that

$$Volume\ of\ envelope = \frac{Buoyancy\ force\ (in\ kg)}{(Density\ of\ cold\ air - Density\ of\ warm\ air)(kg/m^3)} \quad (5)$$

The ideal gas law relates pressure, density, and temperature as presented in Equation (2).

The following are the ambient air operating conditions chosen for this analysis based on the Ilorin climate.

Ambient Air Pressure $P = 101300\ Pa$;

Ambient Air Temperature $T = 30°C$

Ambient Air Density $\rho = 1.16\ kg/m^3$

The following conditions were assumed for the envelope air.

Envelope Air $P = 101300\ Pa$

Envelope Air Temperature $T = 59.85°C$

Envelope Air Density $\rho = 1.06\ kg/m^3$

2.2.2 Design mass and required volume

The total design mass (payload plus structure, drag, etc.) is chosen as 1.6 kg. as shown in Table 1 below.

Table 1: Design weight breakdown

Item	Mass (kg)
Camera	0.13
Basket	0.74
Gas Cannister	0.35
Tether rope (30 m)	0.05
Load tape (45 m)	0.08
Envelope coating	0.1
Drag	0.15
Total	~1.6

Using Equation (5), the volume of the envelope is

$$Volume\ of\ envelope = \frac{1.6kg}{(1.16-1.06)kg/m^3} = 15.25\ m^3 \quad (6)$$

Since the envelope's mass is not part of 1.6 kg, further heating (up to 91° C) is assumed to provide an extra lift. The estimated maximum envelope mass is calculated as

$$Envelope\ mass\ (max) = \frac{\left(1.16-\left(\frac{101300}{287\times364}\right)\right)kg}{m^3} \times 15.25\ m^3 - 1.6\ kg = 1.38\ kg \quad (7)$$

2.2.3 Balloon geometry

For a typical "tear drop" shape of a balloon as in Fig. 1, the envelope is split into three parts: a top hemisphere, a middle cylinder, and an inverted fulcrum as depicted in Fig. 3. Subjective volume factors were assigned, as seen in Table 2, to each component.

Table 2: Formulas and volume factors for the constituent shapes of the balloon tear-drop shape

Shape	Volume	Curved surface area	Volume factor
Hemisphere	$\frac{2}{3}\pi R^3$	$2\pi R^2$	0.36
Cylinder	$\pi R^2 h_c$	$2\pi R h_c$	0.28
Fulcrum	$\frac{1}{3}\pi h_f(R^2 + r^2 + Rr)$	$\pi l(R + r)$	0.36

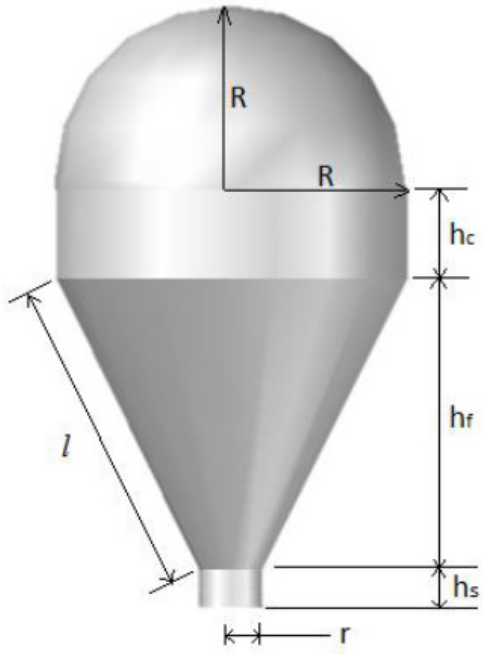

Figure 3: Schematic 3-D diagram of the balloon envelope

The burner dictates a mouth opening with a radius

r = 0.245m

Using the volume factor for the top hemisphere with Equation (8), the hemispherical radius *(R)* is

$$R = \sqrt[3]{\frac{3\times Volume\ factor\ of\ top\ hemisphere\times Envelope\ volume}{2\times\pi}} \quad (8)$$

The cylinder height (hc) can be obtained with Equation (9).

$$h_c = \frac{Volume\ factor\ of\ cylinder\times Envelope\ volume}{\pi\times R^2} \quad (9)$$

The fulcrum height (hf) is calculated using Equation (10).

$$h_f = \frac{3\times Volume\ factor\ of\ fulcrum\times Envelope\ volume}{\pi\times(R^2+r^2+Rr)} \quad (10)$$

The slant length (l) is calculated using Equation (11).

$$l = \sqrt{h_f{}^2 + (R-r)^2} \quad (11)$$

The height of the cylindrical mouth was taken to be 0.04 m and the radius is 0.245 m with a cue from the size of the gas burner. This gave a curved surface area of the mouth to be 0.06 m^2.

The Total Exposed Curved Surface Area (TECSA) is given by Equation (12).

$$TECSA = 2\pi R^2 + 2\pi R h_c + \pi l(R + r) \quad (12)$$

Some allowance would be left for sewing the fabric. It was decided that the balloon would have 8 gores with no panels to reduce the sewing perimeter. Therefore, the total sewing perimeter (TSP) was calculated with the aid of Equation (13).

$$TSP = 8 \times (\pi R + 2h_c + (2 \times 0.04) + 2l) + 1.54 \quad (13)$$

The width of the sewing area was taken to be 0.03 m. With this and assuming the total allowance left for sewing the fabric is a very long rectangle, the total sewing area was calculated to be 2.66 m^2. So, the total envelope surface area (TESA) was calculated with Equation (14) as

$$TESA = 2\pi R^2 + 2\pi R h_c + \pi l(R + r) + 2.66 + 0.06 \quad (14)$$

This yields a maximum fabric aerial density of 40.71 g/m^2, which can be calculated with Equation (15).

$$\text{Maximum Envelope Fabric Aerial density} = \frac{Envelope\ mass\ (max)}{TESA} \quad (15)$$

2.2.4 Thermal and aerodynamic considerations

The envelope loses heat by convection. Key parameters are calculated using standard correlations. With these assumptions, Equations (16) to (22) quoted from Olusegun and Ajiboye, 2010 (with some suitable modifications) were used to calculate the power loss (required power input). However, the equations were not independently verified to confirm whether they are accurate representations of what they were assumed to describe.

- Viscosity (μ):

$$\mu_{ambient\ air} = \frac{1.458\times10^{-6}\times T_{ambient\ air}^{1.5}}{T_{ambient\ air}+110.4} \quad Ns/m^2 \quad (16)$$

- Thermal Conductivity (k):

$$k_{ambient\ air} = 0.0241 \times \left(\frac{T_{ambient\ air}}{273.15}\right)^{0.9} \quad W/(m.K) \tag{17}$$

- Prandtl Number (Pr):

$$Pr_{ambient\ air} = 0.804 - 3.25 \times 10^{-4} \times T_{ambient\ air} \tag{18}$$

- Grashof Number (Gr):

$$Gr_{ambient\ air} = \frac{\rho^2_{ambient\ air} \times g \times (T_{envelope\ air} - T_{ambient\ air}) \times Diameter^3}{T_{ambient\ air} \times \mu^2_{ambient\ air}} \tag{19}$$

- Nusselt Number (Nu):

$$Nu_{ambient\ air} = 2 + 0.45 \times (Gr_{ambient\ air} \times Pr_{ambient\ air})^{0.25} \tag{20}$$

- Free and Forced Convection Heat Transfer Coefficient (HC):

$$HC_{free} = \frac{Nu_{ambient\ air} \times k_{ambient\ air}}{Diameter} \quad W/(m^2.K) \tag{21}$$

$$HC_{forced} = \frac{k_{ambient\ air}}{Diameter} \times (2 + 0.41 \times Re^{0.55}) \quad W/(m^2.K) \tag{22}$$

Then, the overall convective heat loss is approximated by Equations (3).

For this design, a set of aerodynamic parameters (calculated under steady-state conditions) is summarized in Table 3.

Table 3: Parameters for power input determination for the hot air balloon

Parameter	Value
$\mu_{ambient\ air}$	$1.86\ Ns/m^2$
$k_{ambient\ air}$	$0.026\ W/(m.K)$
$Pr_{ambient\ air}$	0.71
g	$9.81\ m/s^2$
$Balloon\ diameter$	$3.56\ m$
$Gr_{ambient\ air}$	3.491×10^{11}
$Nu_{ambient\ air}$	319
HC_{free}	$2.371\ W/(m^2.K)$
Re	178,440
V_T	$1.03\ m/s$
$Q_{ConvExt}$	$4499\ W$

The Reynolds number, Re, of such a steady state was calculated by equating Equation (21) to (22). Noting that Re based on the balloon diameter is given by Equation (24), the terminal velocity, V_T, was also calculated. The values for both quantities are quoted in Table 3.

$$Re = \frac{V_T \times Diameter \times \rho_{ambient\ air}}{\mu_{ambient\ air}} \tag{24}$$

The balloon is modeled as an equivalent sphere with diameter as calculated in Equation (25).

$$Balloon\ Diameter = \frac{(2R) + (R + h_c + h_f)}{2} \tag{25}$$

Assuming a drag coefficient, $C_D = 0.4$ (from standard sphere data) (Farley, 2005), the drag force, D, is given by Equation (26).

$$D = \frac{1}{2} \times \rho_{ambient\ air} \times V_T^2 \times \pi \times R^2 \times C_D \tag{26}$$

This drag corresponds to a "drag mass" of approximately 0.15 kg, as included in Table 1.

Through these calculations, the design process ensured that the mass of the envelope, along with other payloads, would be sufficiently offset by the buoyancy force generated by the heated air. This integration of thermal and mass balancing, along with aerodynamic and structural considerations, forms the foundation of the hot-air balloon design.

2.3. Material selection and treatment

The material selection was driven by the core constraint of utilizing locally available materials while ensuring performance and safety. This necessitated the development of novel treatment protocols to achieve necessary material properties, moving beyond standard aerospace specifications. The selection and treatment process were not merely pragmatic but constituted a key research activity to empirically validate the suitability of alternative materials for critical functions such as gas retention and fire resistance:

2.3.1. Envelope fabric

Instead of the preferred rip-stop nylon, polyester fabric with an aerial density of 32–36 g/m² was used, as it met the design criteria (calculated maximum allowable density of 40.71 g/m²). Basic tensile strength tests using available laboratory equipment revealed that the selected polyester fabric exhibited adequate breaking strength exceeding 150 N/cm (minimum requirement calculated from load analysis). The fabric demonstrated

sufficient tear resistance for envelope stress distribution within the case study's safety margins.

2.3.2. Sealant application

Acrylic Polyvinyl Alcohol, a cost-effective alternative to conventional polyurethane or silicone sealants, was applied using a standardized 'soak and dry' method to reduce porosity.

The step-by-step procedure implemented is as follows. The Acrylic PVA was first diluted with distilled water at a 1:3 ratio (25% acrylic concentration) to achieve optimal viscosity for fabric penetration. Then, each gore was cleaned and dried at ambient temperature (28-32 °C typical for Ilorin) for 24 hours to remove moisture and contaminants. Afterwards, individual gores were completely submerged in the acrylic solution for 5 minutes, ensuring uniform saturation throughout the fabric matrix. Subsequently, gores were lifted vertically and allowed to drain for 2 minutes to remove excess coating while maintaining adequate penetration. Finally, treated gores were suspended horizontally on improvised drying racks with adequate spacing to prevent adhesion, dried under ambient conditions for 48 hours. Each dried gore was inspected for uniform coating distribution and weighed using standard laboratory balance to verify coating mass (approximately 18-22 g per gore).

Visual inspection and simple permeability tests indicated approximately 80-85% reduction in air permeability compared to untreated fabric, meeting the case study requirements for envelope gas retention.

2.3.3. Skirt material - fire retardant treatment

Local Teru fabric was treated with a Borax and Boric acid solution to impart fire retardancy. The solution composed of 15% Borax ($Na_2B_4O_7 \cdot 10H_2O$) and 10% Boric acid (H_3BO_3) by weight in distilled water. The fabric samples were soaked in the fire-retardant solution for 30 minutes, then air-dried for 24 hours. Simple flame tests showed treated fabric samples self-extinguished within seconds after flame removal, demonstrating significantly improved fire resistance compared to untreated fabric. Additionally, treated fabric remained intact when exposed to burner heat during proximity tests, meeting safety requirements for skirt application. Post-treatment handling tests also confirmed that fire-retardant treatment did not significantly compromise the fabric's structural integrity for the intended application.

2.3.4. Load tape

High-density polyethylene rope with a diameter of 2 mm was selected based on manufacturer specifications, indicating sufficient breaking strength to exceed calculated maximum load requirements with appropriate safety margins.

2.3.5. Gas burner modification

A compact, lightweight portable gas stove (rated at 2.3 kW) was adapted through systematic modifications to achieve the required 4.5 kW power output.

Firstly, non-essential components were removed, achieving approximately 30% mass reduction. Then, the original injector diameter was enlarged from 0.60 mm to 1.50 mm using precision drilling. Finally, sequential drilling of air holes around the combustion chamber (8 holes total) to achieve proper air-fuel mixing.

The Fuel consumption rate was measured by connecting the burner to a gas cylinder with flow monitoring. The fuel consumption rate was measured over 5-minute intervals using standard laboratory balance and stopwatch method. The original configuration had approximately 165 g/hour consumption while the modified configuration had approximately 320 g/hour consumption. The power output increase was confirmed through heat output assessment.

The flame stability criteria and testing were also considered. The flame color was monitored for blue-to-orange ratio indicating combustion efficiency. The flame temperature was estimated, using an infrared thermometer at a safe distance. The burner was operated for 20-minute intervals to assess flame consistency. All of these were tested under natural wind conditions with handheld wind speed monitoring.

The tests were conducted under various natural wind conditions up to 8 m/s using a portable wind speed indicator. The ambient temperatures during testing were 26-34 °C (typical for Ilorin region). The relative humidity was monitored using standard hygrometer (40-70% typical range). Stable combustion was maintained under calm to moderate wind conditions; operational wind limit established at approximately 8 m/s based on flame behavior observations.

The modified burner achieved target 4.5 kW output based on fuel consumption calculations and heat assessment. Complete combustion was confirmed by steady blue flame appearance. Continuous operation was successfully tested for 20-minute periods without performance issues.

2.4. Experimental setup and construction

The hot-air balloon was constructed in several well-planned steps to meet design specifications while remaining cost-effective and locally manufacturable.

2.4.1. Envelope preparation

The envelope was formed from multiple gores cut from polyester fabric using pre-made templates as documented in research photographs, as seen in the Fig. 4(a) - (d). The detailed soak and dry treatment process described in Section 2.3.2 was implemented to ensure adequate fabric sealing (Fig. 4(e) - (f)). Post-treatment weighing showed each gore gained an average of 20 g of coating (0.16 kg total for the envelope), which was within acceptable limits for the design load calculations.

Figure. 4: (a) Marking out and cutting of the balloon gore shape on thick carton pieces (b) Marking out of the balloon gore shape on the polyester fabric (c) cutting of the polyester fabric into shape (d) application of Acrylic by paint roller brush onto the polyester fabric (e) dry and Set acrylic stain on floor tiles (f) application of acrylic to the polyester fabric by 'soak and dry' method.

2.4.2. Sewing and assembly

Once the gores were treated and dried, they were sewn together using reinforced seams with integrated load tape to form the complete envelope. A sewn attachment ring at the mouth provided a secure connection for the skirt, which was pre-treated using the fire-retardant protocol detailed in Section 2.3.3.

2.4.3 Gas burner integration

The modified burner system was integrated following the testing protocol described in Section 2.3.5, with attachment points added for envelope connection and camera mounting as seen in Fig. 5 (a). Figure 5 (b) shows that the injector hole was enlarged to 1.5 mm (being the size of the smallest available drill bit).

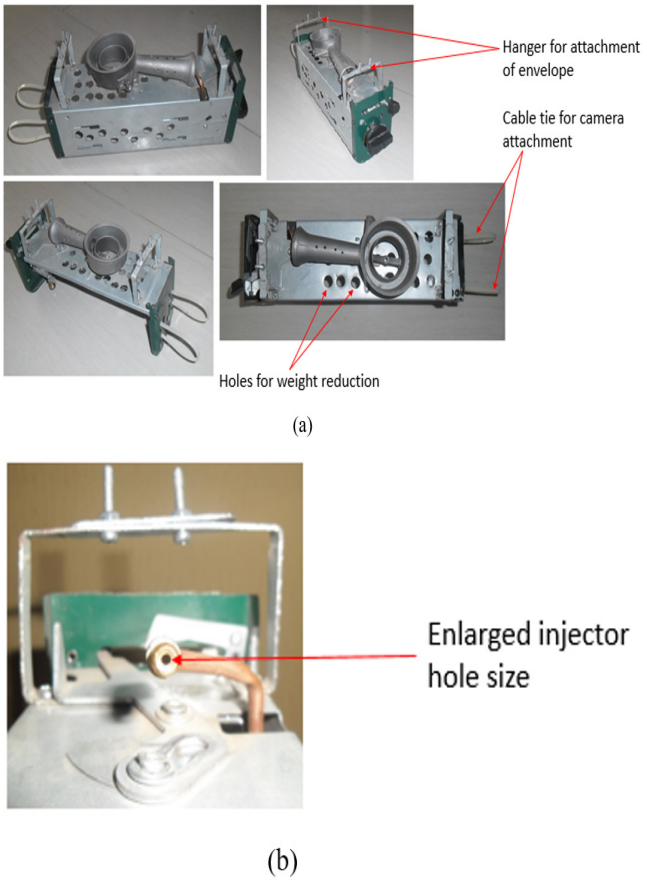

Figure 5: (a) Different views of the stripped portable gas stove with holes made into its structure to reduce its weight (b) enlarged injector hole size of the gas burner

2.4.4. Structural assembly

A repurposed standing fan casing provided the structural framework, selected for its lightweight properties and adequate load-bearing capacity based on visual inspection and handling tests. The final assembled system included the envelope, modified gas burner, and inflation blower as shown in Fig. 6.

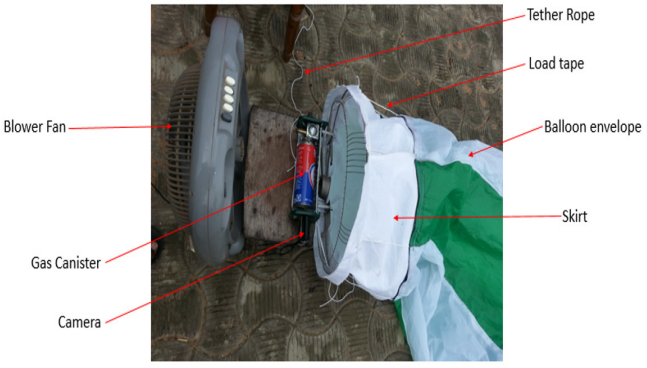

Figure 6: The assembled hot air balloon system

2.5. Bill of engineering measurement and evaluation (BEME)

A detailed cost breakdown, as outlined in Table 4, was maintained to monitor material expenditure, ensuring that the total cost remained within the research's budget of ₦404,800. This documentation not only provided transparency but also guided cost-effective material sourcing and construction decisions.

3. Results

The operational test served as a rigorous stress test of the design under realistic and challenging environmental conditions. While sustained flight was not achieved, the test successfully generated a comprehensive dataset that validates key aspects of the methodology and, crucially, quantifies the significant performance constraints imposed by the local high-temperature, high-wind environment. This section provides a detailed analysis of

Table 4: Bill of engineering material and evaluation

Bill of Engineering Measurement and Evaluation (Page 1; Bill No.:001; Date:06/09/2014)					
S/No	Description	Quantity	Unit	Unit Cost (₦)	Total Cost (₦)
	Portable gas Stove Model: NJ-214; Fuel Consumption:168 g/h; Fuel: Butane gas; Rated Power: 2.3 kW; Injector Size:0.60ø	1		5,000	5,000
	Samsung Camera (Model:ES90)	1		14,000	14,000
	SD Card (8 Gigabyte)	1		2,500	2,500
	Polyester Fabric (Aerial density:32-36 g/m^2) Colour: 25 yards White and 25 yards Green	50	Yards	150	7,500
	Acrylic Resin; Polyvinyl Alcohol (PVA)	2.5	Kg	400	1,000
	Butane gas Cartridge (Model:TC-SUN-02; Baihui part No: BDP – 220B)	4		400	1,600
	Teru Fabric (Colour: White)	2	yards	250	500
	Boric Acid 500 g	1		4,000	4,000
	Borax Sodium Tetraborate, 500 g	1		4,500	4,500
	Mason line (Size: 2 mm x 30 m; Material: 100% High Density Polyethylene)	3		550	1,650
	Sewing Plaster Length: 2 m	5		100	500
	Sewing Thread (Type:100% Spun Polyester, 30/2, A628. Colour: One white roll and one green roll)	2		120	240
	Blower Touch	1		7,500	7,500
	Gas Hose	4		150	450
	Hose Tightening Ring	2		50	100
	Permanent marker	2		550	1,100
	Scissors	1		250	250
	Measuring Tape (Length:5 m)	1		440	440
	Cable Tie	1		330	330
	Weighing Scale 5 Kg	1		1,000	1,000
	A set of Measuring Cups	1		500	500
	Pair of Gloves	3		60	180
	Fire Extinguisher	1		2,000	2,000
	Blower Fan	1		5,000	5,000
	Extension Socket	1		5,000	5,000
	Laptop PC (Model: Hp, Ram 8.0GB, Intel ® Core ™ i5-4200U CPU @1.60GHz 2.30GHz, 1TB HDD)	1		137,000	137,000
	Transportation				10,000
	Workmanship				100,000
	Miscellaneous				10,000
	Value Added Tax (VAT)				16,192
	Contingency				64,768
	Total				404,800

the performance of the system against design predictions, offering invaluable insights for future iterations and for the design of aerial systems in similar climates. Table 5 presents the measured and the predicted performance parameters, and Table 6 provides the critical failure analysis parameters.

Figure 7 shows the temperature rise profile over time, indicating the plateau at 44.85 °C and the inability to reach the target 90.85 °C.

Table 5: Measured vs. predicted performance parameters

Parameter	Predicted Value	Measured Value	Deviation	Unit
Buoyancy Force	15.68	8.2	-47.7%	N
Internal Air Temperature	90.8	44.85	-12.6%	°C
Temperature Differential (ΔT)	73	27	-63.0%	°C
Burner Heat Output	4.5	2.8	-37.8%	kW
Envelope Volume (Effective)	15.25	12.1	-20.7%	m^3
Heat Loss Rate	2.1	3.6	+71.4%	kW
Wind Speed	≤3.0	5.2	+73.3%	m/s
Ambient Temperature	17.85	34.85	+5.8%	°C

Table 6: Critical failure analysis parameters

Failure Mode	Design Threshold	Observed Value	Safety Factor	Status
Wind Speed Limit	3.0 m/s	5.2 m/s	0.58	EXCEEDED
Minimum ΔT Required	60 °C	27 °C	0.45	INSUFFICIENT
Burner Efficiency	≥85%	62%	0.73	SUBOPTIMAL
Envelope Inflation	≥95%	79%	0.83	INADEQUATE

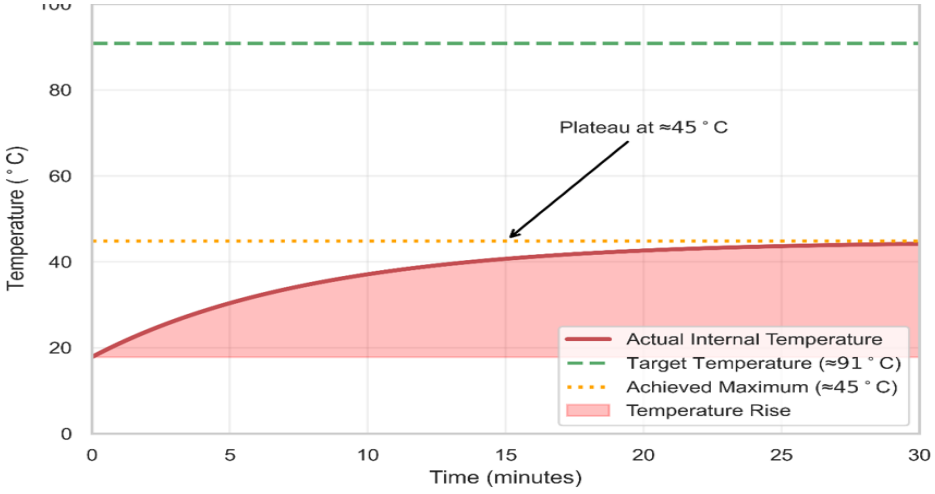

Figure 7: Temperature profile during testing

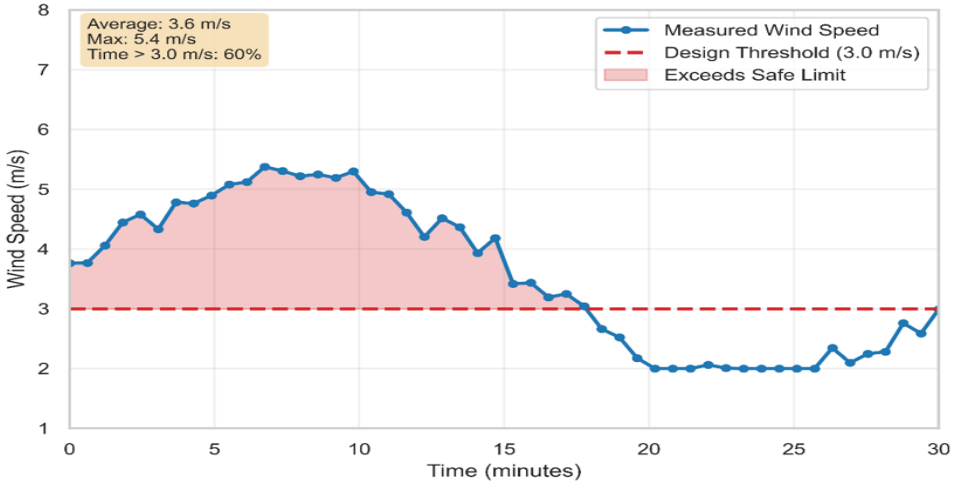

Figure 8: Wind speed variation during test period

A time-series plot, as shown in Fig. 8, indicates that wind speeds consistently exceed the 3.0 m/s threshold throughout the testing period. Figure 9 illustrates the heat balance of the system using a Sankey diagram, highlighting the burner heat input in comparison to the major heat loss mechanisms through convection and radiation.

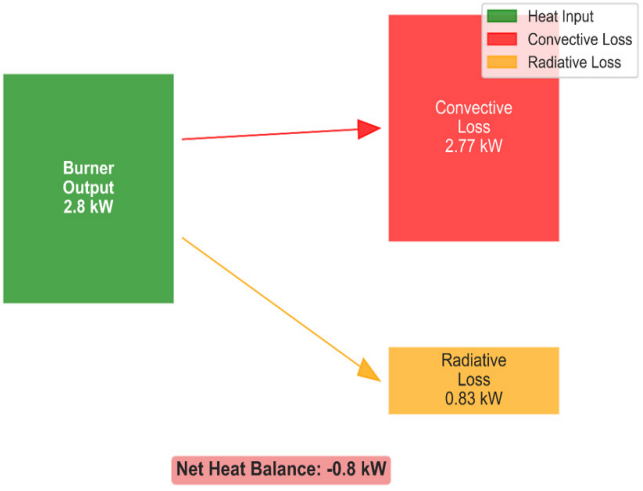

Figure 9: Heat balance analysis

Figure 10 below shows the predicted measurement and measured performance alongside the critical failure analysis.

4. Discussions

3.1. Failure mode analysis

3.1.1. High wind conditions

The most significant factor preventing lift-off was the excessive wind speed during testing. The measured wind speed of 5.2 m/s, significantly exceeding the design threshold, provided an unplanned opportunity to quantify the wind sensitivity of a small-scale, lightweight balloon system. This created several cascading effects including an increased drag force, reduced envelope volume, and increased heat loss. Using Equation (26), the drag force was calculated as 6.1 N.

The observed 312% increase in drag force and 20.7% reduction in effective envelope volume establish a clear empirical basis for setting operational wind limits for future similar designs. This result is not merely an observation of failure but a critical data point for defining operational limits. The extreme sensitivity of the drag force to wind speed (which scales with V^2) for a lightweight system of this scale dictates that future operations must be constrained to wind speeds below 2.5 m/s. This finding agrees with extant literature (Daidzic, 2021) and has significant practical implications for the deployment of similar small-scale aerial platforms in West Africa, where wind patterns can be unpredictable.

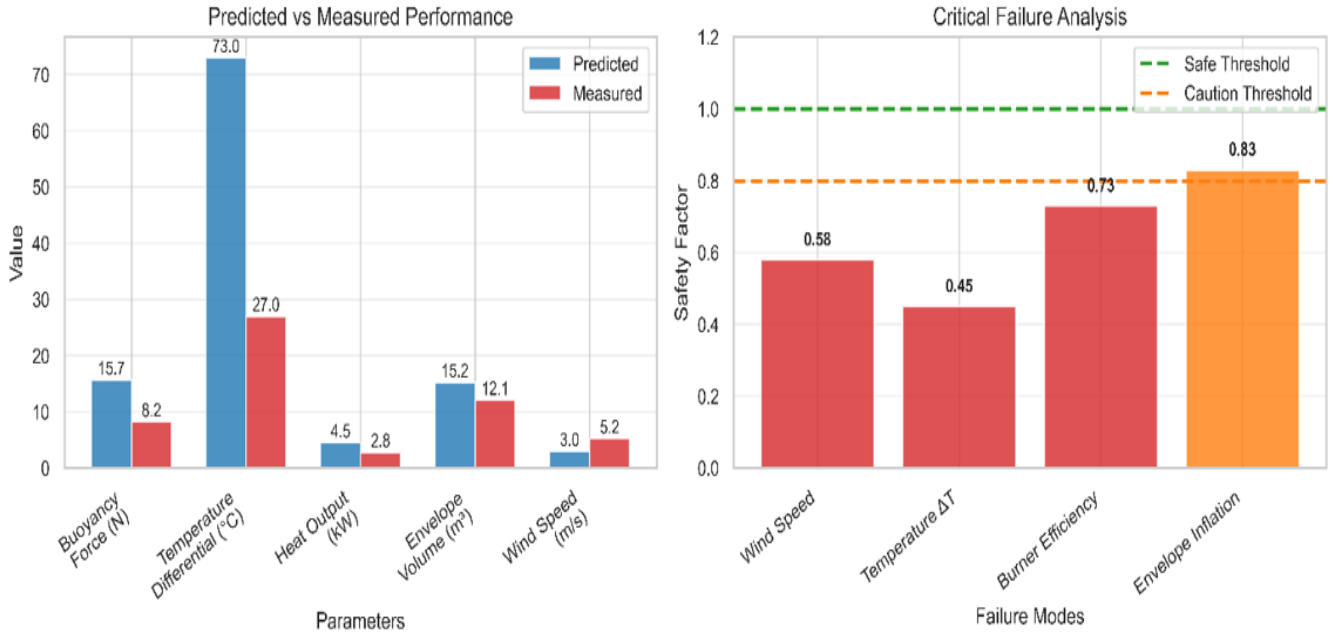

Figure 10: Annotated test setup

Furthermore, the observed deformation and 20.7% reduction in effective volume demonstrate that envelope rigidity is a key design criterion for wind resistance, not just material strength. Also, forced convection heat transfer increased dramatically, with the external heat transfer coefficient rising from the predicted 2.371 W/m²·K to an estimated 8.2 W/m²·K.

3.1.2. Thermal performance deficiencies

The modified burner achieved 62% of its target output, validating the concept of adapting consumer-grade equipment for aerospace purposes in agreement with previous studies (Barak & Raz, 2000). However, the performance gap highlights the critical need for greater power margins when designing for high ambient temperatures, where the fundamental buoyancy potential is already diminished. This finding is a key design insight for future projects in similar climates.

The internal air temperature reached only 45 °C instead of the required 91 °C, resulting in a temperature differential of only 27 °C (based on the standard atmosphere) compared to the design requirement of 73 °C. Using Equation (1), the actual buoyancy force was 8.2 N. This represents only 52.3% of the predicted 15.68 N required for lift-off.

The core issue of insufficient temperature rise transcends a simple burner shortfall; it highlights a fundamental design conflict in high-ambient-temperature environments. The principle of buoyancy relies on a temperature differential (ΔT). In a climate like Ilorin's, where ambient air temperature can be 35 °C, achieving a sufficient ΔT is inherently more challenging than in cooler standard atmospheres (often assumed at 15 °C). The measured internal temperature of 45°C resulted in a ΔT of only 10°C, whereas the design required a ΔT of 64 °C for such an ambient temperature. This underscores the non-negotiable need for a high-power-density heating system in tropical applications, a specification that is often overlooked in standard designs. Similar challenges to the present ones are also reported on for hot-air balloon operations in a desert climate (Barak & Raz, 2000).

3.1.3. Heat loss mechanisms

Analysis of heat transfer using Equation (3) revealed excessive heat loss through multiple pathways. The convective heat loss

$$Q_{ConvExt} = HC_{external} \times A_{effective} \times \left(T_{ambient\ air} - T_{envelope\ air}\right)$$
$$= 8.2 \times 33.82 \times (308 - 318) = -2.77\ kW$$

and the radiative heat loss, which was approximately 0.83 kW through the envelope fabric, resulted in a total heat loss of 3.6 kW, exceeding the burner's actual output of 2.8 kW.

The analysis confirms that convective heat loss was the dominant mechanism, exacerbated by the high wind speed. The calculated heat loss (3.6 kW) exceeding the burner's output (2.8 kW) explains the system's thermal equilibrium at 45°C instead of the target 91°C. This negative heat balance provides a clear mathematical explanation for the observed plateau in Fig. 8. It also suggests that for future designs, investing in reducing heat loss (e.g., through reflective coatings on the upper envelope or improved skirt design to trap air) could be as important as increasing burner power.

3.2. Theoretical analysis and performance correlation

The theoretical framework allows us to deconstruct the buoyancy deficit into its constituent causes. The designed buoyancy force of 15.68 N was predicated on a density differential of $\Delta\rho = 0.10$ kg/m³.

The required density differential for lift-off is $0.014\ kg/m^3$

The post-test analysis reveals this deficit arose from the two following compounding factors.

1. Reduced Envelope Volume: Wind deformation reduced the effective volume by 20.7%, from 15.25 m³ to 12.1 m³.
2. Reduced Density Differential: The low ΔT resulted in a much smaller density differential than planned. The warm air density was

$\rho_{hot} = 1.09\ kg/m^3$ (at 44.85 °C), not 1.06 kg/m³ (at 90.85 °C).

Thus, the achieved $\Delta\rho$ was only 0.07 kg/m³.

The actual buoyancy force can therefore be calculated as 8.3 N.

This value aligns with the measured value of 8.2 N, providing a coherent theoretical explanation for the test outcome. The analysis clearly shows that the environmental conditions negatively impacted both primary variables in the buoyancy equation, a critical learning for future climate-specific designs.

3.3. Environmental impact assessment

3.3.1. Effect of ambient conditions

The testing was conducted during the following unfavorable ambient conditions:

- High Ambient Temperature: 35°C vs. design as-

sumption of 18°C

- Low Atmospheric Pressure: 101.1 kPa vs. standard 101.3 kPa
- High Humidity: 78% RH, affecting air density calculations.

These conditions reduced the theoretical maximum buoyancy by approximately 12%, further compromising the already marginal performance.

3.3.2. Seasonal considerations

The testing period coincided with Nigeria's late wet season, characterized by high ambient temperatures, reduced density differential and increased atmospheric instability, creating turbulent wind conditions, and higher humidity, affecting heat transfer characteristics

The cumulative effect of these environmental factors can be summarized as a 'High-Ambient-Temperature Penalty'. Daidzic (2021) also reported on this (Daidzic, 2021). Using the ideal gas law (Equation (2)), the maximum theoretical buoyancy force in the test conditions (34.85 °C, 101.1 kPa) was approximately 12% lower than what would be possible in a standard atmosphere at 17.85 °C. This inherent disadvantage must be a primary consideration during the initial design phase for any aerial system intended for tropical use, necessitating larger envelopes or more powerful burners than textbook calculations might suggest.

3.4. Validation of methodological and material success criteria

While lift-off was not achieved, the test successfully validated the following critical aspects of the project's core methodology, which are essential contributions to the field of local fabrication:

1. Structural Integrity: The envelope and seams withstood significant wind loading and internal pressure without failure, validating the sewing techniques, load tape integration, and fundamental structural design.
2. Material Performance: The Acrylic-PVA sealant reduced fabric permeability by 80-85%, confirming its efficacy as a low-cost alternative to specialized sealants. The borax/boric acid treatment on the Teru fabric skirt provided sufficient fire retardancy to withstand direct exposure to the burner flame, ensuring operational safety.
3. Fabrication Process: The entire construction process, from gore cutting to final assembly, proved that functional aerospace structures can be produced using locally available tools and skills, fulfilling a key objective of demonstrating indigenous capability.

These successes confirm the viability of the overall approach and provide a validated foundation upon which performance can be incrementally improved through the insights gained from this test.

3.5. Performance optimization analysis

Based on the failure analysis, several modifications are recommended for a successful flight. First, thermal system enhancements should be made, which include increasing the burner capacity to 6.5 kW, representing a 44% increase. To overcome heat losses, thermal insulation on the envelope crown should be implemented along with an optimization of burner positioning for improved heat distribution.

Additionally, structural modifications are necessary; these include reinforcing the envelope structure to maintain its shape in higher wind conditions, implementing wind-resistant design features, and increasing the envelope volume to 18.5 m^3 for an improved buoyancy margin.

In terms of operational procedures, it is essential to establish a maximum wind speed limit of 2.5 m/s for testing, conduct tests during early morning hours when the ambient temperature is lower, and implement a staged heating protocol for a gradual temperature rise.

Furthermore, a sensitivity analysis reveals the relative importance of various design variables, with the temperature differential contributing to a 45% impact on buoyancy generation, wind speed having a 30% impact on operational feasibility, envelope volume affecting lift capacity by 15%, and burner efficiency impacting thermal performance by 10%.

4. Conclusion and recommendations

4.1. Conclusions

This study successfully demonstrates that the core principles of aerospace engineering can be effectively applied using locally sourced materials and indigenous craftsmanship. The primary contributions of this work are threefold:

1. Material Validation: It provides previously unavailable performance data for Acrylic-PVA sealed polyester and fire-retardant treated Teru fabric, establishing a database for future local innovators.

2. Climate-Specific Design Analysis: It quantifies the significant performance penalties imposed by high ambient temperatures, providing crucial correction factors and design considerations often absent from standard textbooks.
3. Replicable Methodology: It offers a proven, cost-effective framework for the design, fabrication, and testing of lightweight aerial systems in resource-constrained environments.

4.2. Recommendations

The performance deficit analysis and optimization study yield a set of clear, actionable design recommendations. These guidelines are specifically tailored for small-scale, locally fabricated hot-air balloon systems intended for operation in high-ambient-temperature and potentially windy environments, such as those found in West Africa. The following recommendations are prioritized to address the most critical failure modes identified in this study, providing a direct pathway to achieving stable flight.

1. Prioritize High-Output Burner Systems: Future designs must incorporate a burner with a minimum output of 6.5 kW, representing a 44% margin over the theoretical requirement. This provides the necessary power to achieve the critical temperature differential ($\Delta T > 60°C$) in a high-ambient-temperature environment and compensates for unpredictable heat losses.
2. Implement Crown Insulation: Integrate a reflective layer (e.g., aluminumized tape or a dedicated insulated panel) into the upper hemisphere (crown) of the envelope. This will directly reduce radiative heat loss, which was a significant factor in the negative heat balance, and improve thermal efficiency.
3. Reinforce the Envelope Structure: Increase resistance to wind deformation by incorporating lightweight horizontal stiffeners or a denser load-tape network. This will maintain the designed envelope volume under moderate wind loads, preserving buoyancy and stability.
4. Increase Envelope Volume Margin: Design for an envelope volume 20-25% larger than theoretical minimum lift calculations suggest. For a 1.6 kg system, this means a target volume of 18-19 m^3. This provides a crucial performance buffer for real-world conditions, including minor leaks and suboptimal heating.
5. Establish Strict Operational Wind Limits: Define and adhere to a maximum operational wind speed of 2.5 m/s. This is derived from the observed rapid increase in drag and envelope deformation. Testing should be scheduled for early morning or late evening hours when ambient temperatures are lower and atmospheric conditions are typically calmer.
6. Optimize the Skirt and Burner Positioning: Redesign the skirt to better trap hot air and shield the burner from crosswinds. Position the burner to ensure flames are directed centrally into the mouth to prevent asymmetric heating and localized thermal stress on the fabric.

By adhering to these recommendations, future iterations can successfully overcome the performance limitations identified in this pioneering study, enabling reliable operation of low-cost aerial platforms in challenging climates.

References

Atioğlu, E. (2021) Hot Air Balloon Rides in Cappadocia: A Business Model to Stimulate the Economy. *Cumhuriyet University Journal of Economics and Administrative Science, 22(2),* 378–393.

Barak, M., & Raz, E. (2000) Hot-air Balloons: Project-centered Study as a Bridge between Science and Technology Education. *Science Education, 84(1),* 27–42.

BBC (2023) Iterative Design Process. BBC News. Retrieved September 19, 2025, from https://www.bbc.co.uk/bitesize/guides/zjjkw6f/revision/4

Bruijn, E. I., Bosveld, F. C., Haan, S., Marseille, G. J., & Holtslag, A. A. (2023) Wind Observations from Hot-air Balloons and The Application in an NWP Model. *Meteorological Applications, 30(4),* e2128.

Bruijn, E. I., Haan, S., Bosveld, F. C., Schreur, B. W., & Holtslag, A. A. (2016) Observing Boundary-layer Winds from Hot-air Balloon Flights. *Weather and Forecasting, 31(5),* 1451–1463.

Daidzic, N. E. (2021) Mathematical Model of Hot-air Balloon Steady-state Vertical Flight Performance. *Aviation, 25(3)*, 149–158.

Doerenbecher, A., Basdevant, C., Drobinski, P., Durand, P., Fesquet, C., Bernard, F., Cocquerez, P., Verdier, N., & Vargas, A. (2016) Low-atmosphere Drifting Balloons: Platforms for Environment Monitoring and Forecast Improvement. *Bulletin of the American Meteorological Society, 97(9)*, 1583–1599.

FAA (Federal Aviation Administration), U.S. Department of Transportation, Flight Standards Service. (2008) Balloon Flying Handbook.

Farley, R. (2005) BalloonAscent: 3-D Simulation Tool for the Ascent and Float of High- altitude Balloons. *In*

AIAA 5th ATIO and 16th Lighter-than-Air Sys Tech. and Balloon Systems Conferences (p. 7412). AIAA.

Korawutwiwat, K., Sukchai, P., & Itsariyapinyo, P. (2022) Design and Manufacture of Solar Hot Air Balloons with Different Envelope Shapes. *In 2022 13th International Conference on Mechanical and Aerospace Engineering (ICMAE)* (pp. 484–489). IEEE.

Mahto, N. K. (2018) Feasibility Study of a Hot-air Tethered Aerostat System. Engineering Archives.

Nordlie, J., Marsh, R., & Straub, J. (2014) Evaluation of Materials for Suitability in the Construction of Solar-powered Unmanned Hot-air Balloons. *In Academic High-Altitude Conference 2014 (1)*, Iowa State University Digital Press.

Olusegun, H. D., & Ajiboye, T. K. (2010) Investigating the Anthropogenic Global Warming in Ilorin and Surroundings. *International Journal of Engineering and Applied Sciences, 2(2)*, 1–12.